The Lifetimes of Plasma Structures at High Latitudes

Magnus F Ivarsen[1], Yaqi Jin[1], Andres Spicher[1], Wojciech Miloch[1], and Lasse B N Clausen[1]

[1]Department of Physics, University of Oslo, Oslo, Norway

Key Points:

- The ratio of E-region to F-region conductance is an accurate predictor of F-region polar cap plasma diffusion.
- During local winter, diffusion is virtually absent in small-scale (~ 1 km) plasma structures.
- F-region small-scale plasma structure lifetimes in the central polar caps range from 30 minutes to 90 minutes.

Corresponding author: Magnus F Ivarsen, `m.f.ivarsen@fys.uio.no`

Abstract

We present an investigation of small- to intermediate-scale (< 4 km) polar cap plasma structure lifetimes. We analyze both data from ionospheric models (International Ionosphere Reference model and Mass Spectrometer Incoherent Scatter model) and from in-situ observations from the Swarm satellite mission (the 16 Hz Advanced Plasma Density data set). We find that the theoretical prediction that E-region conductance is a predictor of F-region polar cap plasma structure lifetimes is indeed supported by both in-situ-based observations and by ionospheric models. In-situ plasma structure lifetimes correlate well with the ratio of E- to F-region conductance. We present explicit predictions about small scale (~ 1 km) structure lifetimes, which range from 30 minutes during local summer to around 90 minutes during local winter. We go on to discuss anomalous diffusion in the ionosphere, and suggest a way to bridge the gap between theory and observations on the topic of ionospheric plasma diffusion.

1 Introduction

In the high-latitude ionosphere, the primary source regions for plasma structuring tend to be located in the dayside cusp and the nightside auroral oval, where electron precipitation is abundant (Kelley et al., 1982). The large-scale polar convection pattern then causes the structured plasma to travel anti-sunward through the polar cap (Dungey, 1961; Cowley & Lockwood, 1992). In fact, the transport of irregularities from particle precipitation-driven source regions into the polar cap proper is an essential reason for the observed polar cap plasma structures (Cowley, 2000), although alternative sources of structuring inside the polar cap proper exist, such as the gradient drift instability mechanism (e.g., Tsunoda, 1988). Without an irregularity production source, the lifetime of a given plasma structure entering the polar cap is an indicator of the effectiveness with which the plasma structures are diffusing into the surrounding plasma. Indeed, Jin et al. (2017) found that occurrence of plasma irregularities drop significantly when plasma leaves the cusp region.

The occurrence of plasma irregularities in the high-latitude regions is in general subject to strong seasonal dependencies (Heppner et al., 1993; Ghezelbash et al., 2014; Prikryl et al., 2015; Jin et al., 2018). In general, local winter is accompanied by an increase in observed plasma irregularities. Additionally, the occurrence rate for the large-scale polar cap patches is higher during local winter (Foster, 1984; Schunk & Sojka, 1987; Coley & Heelis, 1998; Wood & Pryse, 2010; Spicher et al., 2017). Recently, Ivarsen et al. (2019) found clear evidence for the seasonal dependency plasma structure diffusion, on average for scales < 5.8 km, concluding that local season is a powerful indicator for the existence of plasma irregularity dissipation.

Pressure gradients in plasma cause plasma structures to diffuse into the surrounding plasma (Vickrey & Kelley, 1982). In radial structures, plasma distributed in a long column with an axial external magnetic field applied — assuming rotational symmetry — is only subject to radial, or perpendicular diffusion. Theoretically, in this plasma, ions and electrons diffuse individually (Moisan & Pelletier, 2012). This creates a charge-induced (ambipolar) electric field, which in turn serves to decelerate the diffusion of the faster-diffusing species, and accelerate the slower-diffusing species (Moisan & Pelletier, 2012). The value of the ambipolar electric field then controls the rate of diffusion of plasma structures in the F-region. In a seminal article, Vickrey and Kelley (1982) showed that, theoretically, the height-integrated ionospheric Pedersen conductivity controls the ambipolar electric field, and thus also the rate of F-region plasma diffusion. This mechanism gives rise to the observed seasonal dependency of plasma structure abundance. The equation expressing the height-integrated perpendicular diffusion coefficient in the F-region polar cap reads (Vickrey & Kelley, 1982),

$$\mathcal{D}_\perp = \frac{\Sigma_i^F}{\Sigma_i^F + \Sigma_e^F + \Sigma_i^E + \Sigma_e^E} \left(\mathcal{D}_{\perp,e} - \mathcal{D}_{\perp,i}\right) + \mathcal{D}_{\perp,i}, \tag{1}$$

where Σ_j^k is the height-integrated Pedersen conductivity for the regions $k = E, F$, and $\mathcal{D}_{\perp,j}$ is the height-integrated perpendicular diffusion coefficient, both for species $j = i, e$. In reaility, the Pedersen current is primarily carried by ions, and so the height-integrated Pedersen conductivity can be defined in terms of the ion conductivity only, $\Sigma^k \approx \Sigma_i^k$. With this simplification, it is now instructional to rewrite Eq. (1) in terms of the dimensionless variable Σ^E/Σ^F,

$$\mathcal{D}_\perp = \frac{1}{1 + \Sigma^E/\Sigma^F} \left(\mathcal{D}_{\perp,e} - \mathcal{D}_{\perp,i}\right) + \mathcal{D}_{\perp,i}. \tag{2}$$

In Eq. (2) there are two asymptotes, $\mathcal{D}_{\perp,e}$ and $\mathcal{D}_{\perp,i}$ for low and high values of Σ^E/Σ^F respectively. In other words, a strengthening of Pedersen conductivity in the E-region as opposed to the F-region weakens the ambipolar electric field, causing F-region plasma to diffuse at the high ion perpendicular diffusion rate instead of the balanced ambipolar diffusion rate [the applied magnetic field causes ion rates to be much higher than the electron rates, the reverse of the situation without such a magnetic field (Moisan & Pelletier, 2012)]. Incident sunlight photo-ionization, which typically causes the E-region conductivity, displays a strong seasonal dependence in the polar cap, where sunlight is absent for the winter months. This is the primary driver for observed seasonal dependencies in polar cap plasma irregularity dynamics (Basu et al., 1988; Kelley et al., 1982; Vickrey & Kelley, 1982; Kivanc & Heelis, 1998; Milan et al., 1999; Danskin et al., 2002; Jin et al., 2018).

Let us now turn to the subject of an observable quantity related to the perpendicular diffusion coefficient: structure lifetime. In general, the time scale associated with a diffusion process adheres to the following equation (Huba & Ossakow, 1981; Moisan & Pelletier, 2012),

$$\tau = \frac{\lambda^2}{D}, \tag{3}$$

where λ is a characteristic scale length, and D is the mentioned diffusion coefficient. λ is related to L, the scale of the structure that is undergoing diffusion. However, in the F-region ionosphere, λ is in fact smaller than L (Huba & Ossakow, 1981). The way λ scales with L is only dependent on the properties of the plasma, and the geometry of the situation (Moisan & Pelletier, 2012). Furthermore, small-scale high latitude F-region plasma structures are believed to be generated through instability processes and be the result of the balance between production and decay (Tsunoda, 1988). Consequently, the growth of plasma structures may also effectively increase τ in Eq. (3). τ is also affected by the fact that diffusion is occurring on a range of scales simultaneously. As a structure undergoes diffusion, its scale will increase (this is illustrated with ice cream undergoing heat transfer with its environment in Fig. 1).Consider two adjacent scales, L_1 and L_0, where $L_1 > L_0$. Diffusion processes working on the scale L_1 will then have to effectuate diffusion on structures of scale L_0, the scales of which have increased to L_1 during the course of diffusion. The net result of this scale mixing is an increased τ in Eq. (3).

Unfortunately, the subject of plasma structure lifetime is rarely explicitly addressed, but several in-situ measurements of the diffusion coefficient exists. Gresillon et al. (1992), using data from the SHERPA HF radar, find a diffusion coefficient of 270 $\mathrm{m^2s^{-1}}$ in auroral E-region plasma. The authors attribute this diffusion coefficient to both perpendicular and parallel diffusion. Using the same methods, and likewise utilizing data from the SHERPA HF radar, Villain et al. (1996) performed a statistical study, and found the diffusion coefficient to range from near 0 $\mathrm{m^2s^{-1}}$ to 1000 $\mathrm{m^2s^{-1}}$. This analysis has later

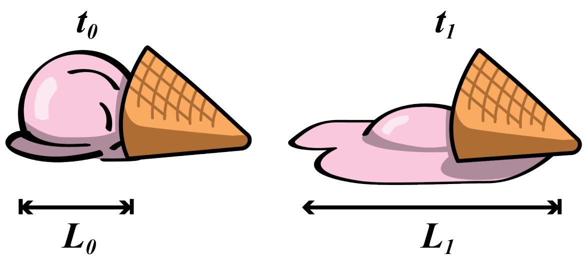

Figure 1. A cartoon showing a structure undergoing diffusion, with the size scale of that structure increasing from L_0 at a time t_0, to L_1 at a time t_1. In this case, the structure is a scoop of ice cream exposed to sunlight undergoing radiation heat transfer with its environment.

been performed on data from several SuperDARN radars; André et al. (2003), also analyzing observations from the auroral region, likewise find diffusion coefficients ranging from near 0 to 1000 m^2s^{-1}. As for explicit values of structure lifetime being reported in the literature, Kelley et al. (1982) conclude that the lifetime of a convecting patch is directly dependent on sun-illumination. Due to chemical recombination, polar cap patches take around 4 hours to decay to 10% of their original density during local summer, while during local winter the required time is around 11 hours (Wood & Pryse, 2010).

The present study is a follow-up investigation based on the findings in Ivarsen et al. (2019), where we intend to investigate high-latitude small- to intermediate-scale ($<$ 4 km) plasma structure lifetimes. By applying both state of the art ionospheric models, and by using data from in-situ satellite missions, we find that the theoretical predictions put forth by Vickrey and Kelley (1982), namely that E-region conductance controls the F-region plasma structure lifetimes in the polar cap, is indeed supported by evidence.

2 Methodology

There are two aspects to the methodology developed in the present study. First, we make an estimate of plasma structure lifetimes in the polar caps based on in-situ data from the Swarm mission. Second, we approach the perpendicular diffusion coefficient using ionospheric plasma models.

2.1 In-situ plasma structure lifetime estimate

Ignoring irregularity production, we can assume that a portion of plasma (e.g., a polar patch) is convecting anti-sunward through the polar cap, that it only undergoes diffusion, and that it diffuses at a constant rate. Our central assumption is then that a satellite orbiting through the F-region ionosphere plasma will, at any given point along the sun-midnight line, encounter plasma that has undergone convection with a constant velocity, and diffusion without further irregularity production.

Using high-resolution (16 Hz) in-situ plasma density from the Swarm mission (Friis-Christensen et al., 2006; Knudsen et al., 2017), we can estimate small-scale plasma structuring using the observed power spectral density of the measured electron density. With a sampling frequency of 16 Hz, we can probe fluctuations for a range of scales down to about 1 km, assuming that the plasma drift velocity is much smaller than the satellite velocity. At high latitudes, Swarm orbit will be almost perpendicular to Earth's magnetic field lines, and so an orbiting satellite will sample field-perpendicular plasma structures.

	Frequency interval	Mean frequency	Mean scale
f_1	[0.4 Hz, 0.6 Hz]	0.5 Hz	14.5 km
f_2	[0.6 Hz, 0.9 Hz]	0.8 Hz	10.0 km
f_3	[0.9 Hz, 1.3 Hz]	1.1 Hz	7.7 km
f_4	[1.3 Hz, 1.9 Hz]	1.6 Hz	4.8 km
f_5	[1.9 Hz, 2.7 Hz]	2.3 Hz	3.4 km
f_6	[2.7 Hz, 3.9 Hz]	3.3 Hz	2.3 km
f_7	[3.9 Hz, 5.6 Hz]	4.7 Hz	1.6 km
f_8	[5.6 Hz, 8.0 Hz]	6.8 Hz	1.1 km

Table 1. The eight frquency intervals used to analyze the 16 Hz plasma density data, and their corresponding plasma structure scale, assuming that plasma flow velocity is negligible compared to spacecraft velocity.

We consider all polar cap passes between noon and midnight made by Swarm A between 15 October 2014 and 1 July 2019. For each overpass, we translate Swarm A travel time to the distance along a straight line connecting noon to midnight,

$$d = (t - t_0)v_S \cos\alpha, \tag{4}$$

where d is the distance travelled by the convecting plasma, v_S is the orbital velocity of Swarm A, α is the angle made by the orbit with respect to the noon-midnight line, t is Swarm A time, and t_0 is the time at which Swarm A approaches the polar cap. We consider polar cap passes where $\alpha < 30°$, and where the satellite is located poleward of $\pm 82°$ at some point during the pass.

Next, we analyze the measured electron density n. In order to look at fluctuations irrespective of the background density, we consider the unitless relative density perturbations,

$$\tilde{n} = \frac{n - \bar{n}_{1m}}{\bar{n}_{1m}}, \tag{5}$$

where n_{1m} is a running median filter with a window size of 1 minute. We perform a power spectral density analysis (PSD) on $\tilde{n}$. Here, we use a simple fast-Fourier transform procedure, after removing the median 30-second bin median, and applying a Hann window to reduce the effect of spectral noise. We use an overlapping bin size of 60 seconds, with a temporal resolution of 1 second. For each bin, we integrate the PSD over eight logarithmically spaced intervals, from 0.4 Hz down to the Nyquist frequency at 8 Hz (shown in Table 1). This quantity, called the root-mean square (RMS), denoted by P_{RMS}, is equivalent to the variance when performed over the entire power spectrum, and represents the power of fluctuations at the scale over which it is integrated. Some density fluctuation powerspectra made using Swarm 16 Hz plasma density exhibit noise in the highest frequencies (Ivarsen et al., 2019). As a precaution, we impose upon the computed RMS values the requirement that, $P_{\text{RMS}} > 4 \times 10^{-7}$, a threshold found after extensive testing.

Following from the assumptions laid down so far, plasma containing fluctuations characterized by P_{RMS} will, once it enters the polar cap, diffuse at a constant rate $\mathcal{D}_\perp$. The time evolution of a diffusion process on P_{RMS} with the time scale τ_S is characterized by the following differential equation (Moisan & Pelletier, 2012),

$$\frac{\mathrm{d}P_{\mathrm{RMS}}}{\mathrm{d}t_c} = -\frac{1}{\tau_S} P_{\mathrm{RMS}}, \tag{6}$$

which has the solution,

$$P_{\mathrm{RMS}}(t_c) = P_{\mathrm{RMS}}(0)\ \exp\left(-\frac{t_c}{\tau_S}\right). \tag{7}$$

In Eqs. (6) and (7), t_c is the plasma convection time and $P_{\mathrm{RMS}}(0)$ is the initial RMS value at the point of entry into the polar cap. Note that we use τ_S to distinguish the structure lifetime from the theoretical decay time τ — as we expect that structure lifetime as estimated in the present study will deviate from theoretical decay time due to irregularity production scale mixing. Now, to convert Swarm orbital distance d along the noon-midnight line (Eq. 4) to plasma convection time, we write $t_c = d/v_c$, with v_c being the plasma convection velocity. In combination with Eq. (4), we then have for the plasma convection time,

$$t_c = \frac{v_S}{v_c} \cos\alpha\ (t - t_0). \tag{8}$$

For each Swarm A orbit between noon and midnight, we store the plasma convection time t_c and the relative density fluctuations P_{RMS} for all eight frequency intervals.

2.2 Modelling the effective perpendicular diffusion coefficient

Our goal is to solve Eq. (1). To this end, we need expressions for the field-perpendicular diffusion coefficients and the Pedersen conductivity height profiles, both of which depend on the collision frequencies between the plasma species. First, we use expressions from Moisan and Pelletier (2012) for collisional plasma interactions ($D_{\perp,j}$ and $\sigma_{\perp,j}$), which are given below. Second, we use values for the collision interaction terms between all charged particles associated with the ion species in the ionosphere, as presented in Schunk and Nagy (1980). Third, we use the International Ionosphere Reference model (IRI) for the ionospheric ion species number densities and plasma temperatures (Bilitza & Reinisch, 2008; Bilitza et al., 2014), the Mass Spectrometer Incoherent Scatter model (MSIS) for the neutral number densities (Picone et al., 2002), and IGRF for the magnetic field strength (Thébault et al., 2015).

The field-perpendicular diffusion coefficient (not height-integrated) from charged particle collisions is defined as (Moisan & Pelletier, 2012),

$$D_{\perp,j} = \frac{D_{0,j}\nu_j^2}{\omega_j^2 + \nu_j^2}, \tag{9}$$

where, $D_{0,j} = k_B T_j / m_j \nu_j$, with k_B the Boltzmann constant, T_j the temperature, $\omega_j = eB/m_j$ the cyclotron frequency, and m_j is particle mass, all for species j. ν_j is the composite collision frequency,

$$\nu_i = \nu_{in}, \tag{10}$$

$$\nu_e = \nu_{en} + \nu_{ei}, \tag{11}$$

where subscripts i, e, n denote ions, electrons, and neutrals respectively. Looking at Eq. (9), we make an important observation. In the F-region ionosphere, $\omega_j \gg \nu_j$, and so by Taylor expansion,

$$D_{\perp,j} = D_{0,j}\frac{\nu_j^2}{\omega_j^2}\left(1 + \frac{\nu_j^2}{\omega_j^2}\right)^{-1} \approx D_{0,j}\frac{\nu_j^2}{\omega_j^2}\left(1 - \frac{\nu_j^2}{\omega_j^2}\right) \approx D_{0,j}\frac{\nu_j^2}{\omega_j^2} \propto B^{-2}, \tag{12}$$

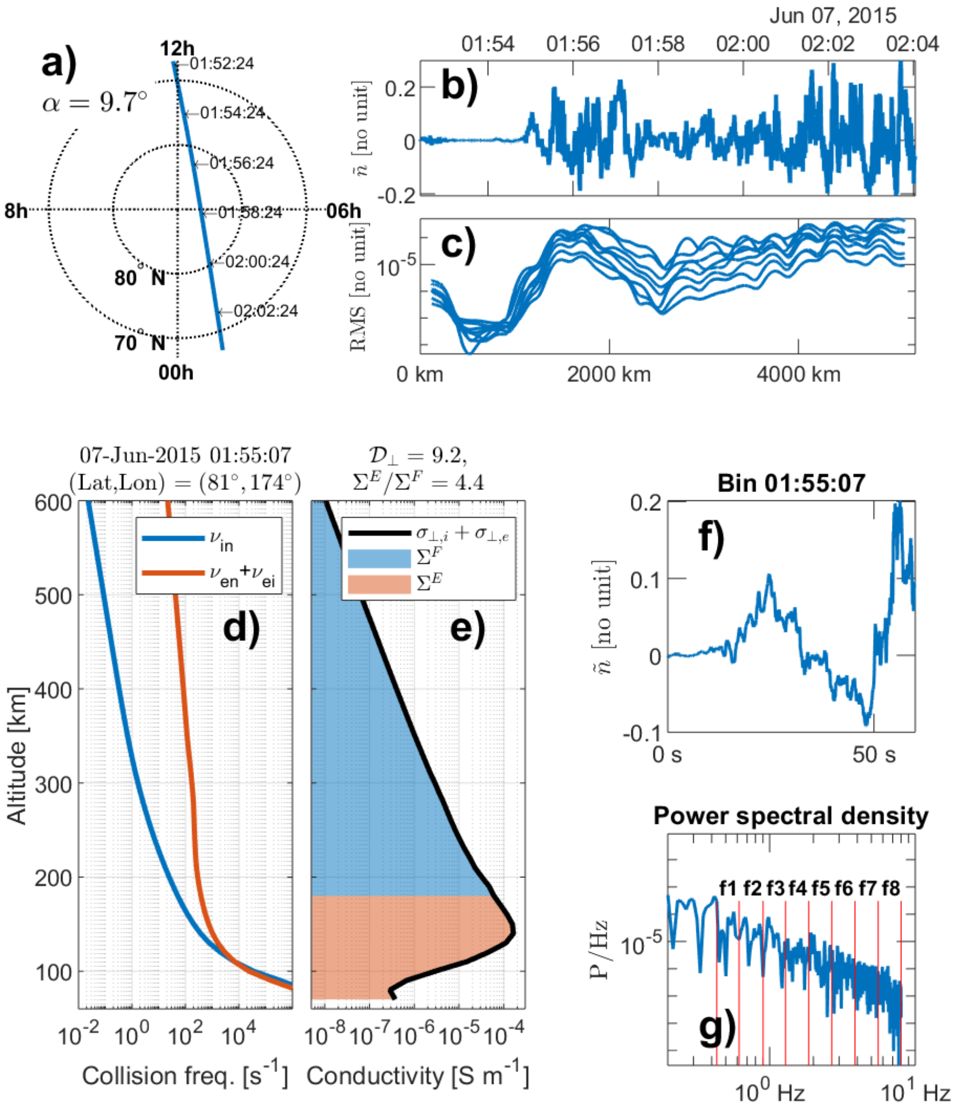

Figure 2. Example of the data analysis performed on the Swarm 16 Hz plasma density data. In panel a), we show Swarm A orbit across the northern polar cap during a 10 minute interval, with α, the angle of the orbit against the noon-midnight line, indicated. In panel b), the 16 Hz relative electron density perturbations for a 12-minute polar cap pass is shown, and in panel c) we show the RMS data plotted against the plasma convection distance d (Eq. 4). The RMS timeseries consists of the integrated PSD over eight frequency intervals, with a running 1-minute window, and a resolution of 1 second. In the lower panels we show the specific analysis of a point in time centered on 7 June 2015, 01:55:07 UT. Panel d) shows the collision frequencies (calcualted using values of the interaction terms from Schunk and Nagy (1980) and MSIS), and panel e) shows the resulting Pedersen conductivity height profiles, with the values of $\mathcal{D}_\perp$ and Σ^E/Σ^F indicated above the plot. Panel f) shows the 1-minute relative density perturbation segment centered on 01:55:07 UT, while panel g) shows the PSD based on this segment, with the eight frequency intervals indicated.

showing that the field-perpendicular diffusion rate due to collisions is inversely proportional to the square of the magnetic field strength.

The ionospheric Pedersen conductivity is given by (Moisan & Pelletier, 2012),

$$\sigma_{\perp,j} = \frac{e^2 n_j}{m_j} \frac{\nu_j}{\omega_j^2 + \nu_j^2} \tag{13}$$

where m_j and n_j is the effective mass and number density for species j respectively.

Next, we need expressions for the height-integrations of Eqs. (12) and (13). The height-integrated perpendicular diffusion coefficient $\mathcal{D}_{\perp,j}$ is defined as (Vickrey & Kelley, 1982),

$$\mathcal{D}_{\perp,j} = \frac{1}{N} \int_{z0}^{\infty} dz \; n_e(z) D_{\perp,j}(z), \tag{14}$$

for species j, and where z signifies the altitude dependency. z_0 is the lowest altitude of the F-region, and N is the height-integrated plasma density, $N = \int_{z_0}^{\infty} dz \; n_e(z)$. Furthermore, the height integrated Pedersen conductivity, or conductance, $\Sigma_j^{E,F}$, is defined as (Vickrey & Kelley, 1982),

$$\Sigma_j^k = \int_k dz \; \sigma_{\perp,j}(z), \tag{15}$$

for species j, and where $k = E, F$ signifies the region, and $\sigma_{\perp,j}(z)$ is the altitude dependent ionospheric Pedersen conductivity (Eq. 13).

Now we are in a position to solve Eq. (1). First, we compute the Pederson conductivity (Eq. 13) for altitudes from 60 km to 600 km, with a 10 km interval. Second, we integrate the resulting height profiles, in addition to the electron density height profiles (from MSES), and evaluate Eq. (14). Third, using the height-integrals in Eqs. (14, 13), we evaluate Eq. (1). For each polar cap pass made by Swarm A, we then calculate and store the values of Σ^E/Σ^F and $\mathcal{D}_\perp$ on a time grid covering the pass.

Fig. 2 documents the data analysis applied to the Swarm 16 Hz plasma density data, along with the application of ionospheric models. Panels a), b) and c) show an entire example polar cap pass, where the orbit, along with the value of α, is shown in panel a), the relative density fluctuation (Eq. 5) is shown in panel b), and the eight RMS timeseries resulting from integrating the PSD over a running 1-minute window are shown in panel c). An example 1-minute segment of the relative density perturbations, and the corresponding PSD, are shown in panels f) and g). Panels d) and e) show height-profiles of the collision frequencies (Eqs. 10, 11), and the Pedersen conductivity (Eq. 13), with the values of Σ^E/Σ^F and $\mathcal{D}_\perp$ indicated.

3 Results

We perform a superposed epoch analysis on the Swarm A polar cap passes. To distinguish between different seasons, we use a 131-day window centered on the December and June solstices, without specifying the year of the polar cap pass. During the period between 14 October 2014 and 30 June 2019, we registered a total of 3366 passes in the northern hemisphere, and 1698 passes in the southern hemisphere. The reason for the large number discrepancy is due to Swarm orbital dynamics: the polar orbit of Swarm A is inclined 2.6 degrees from Earth's geographic axis. Compared to the northern hemisphere, the geomagnetic south pole is further away from the geographic south pole, leading to fewer noon-midnight passes occurring in the southern polar cap.

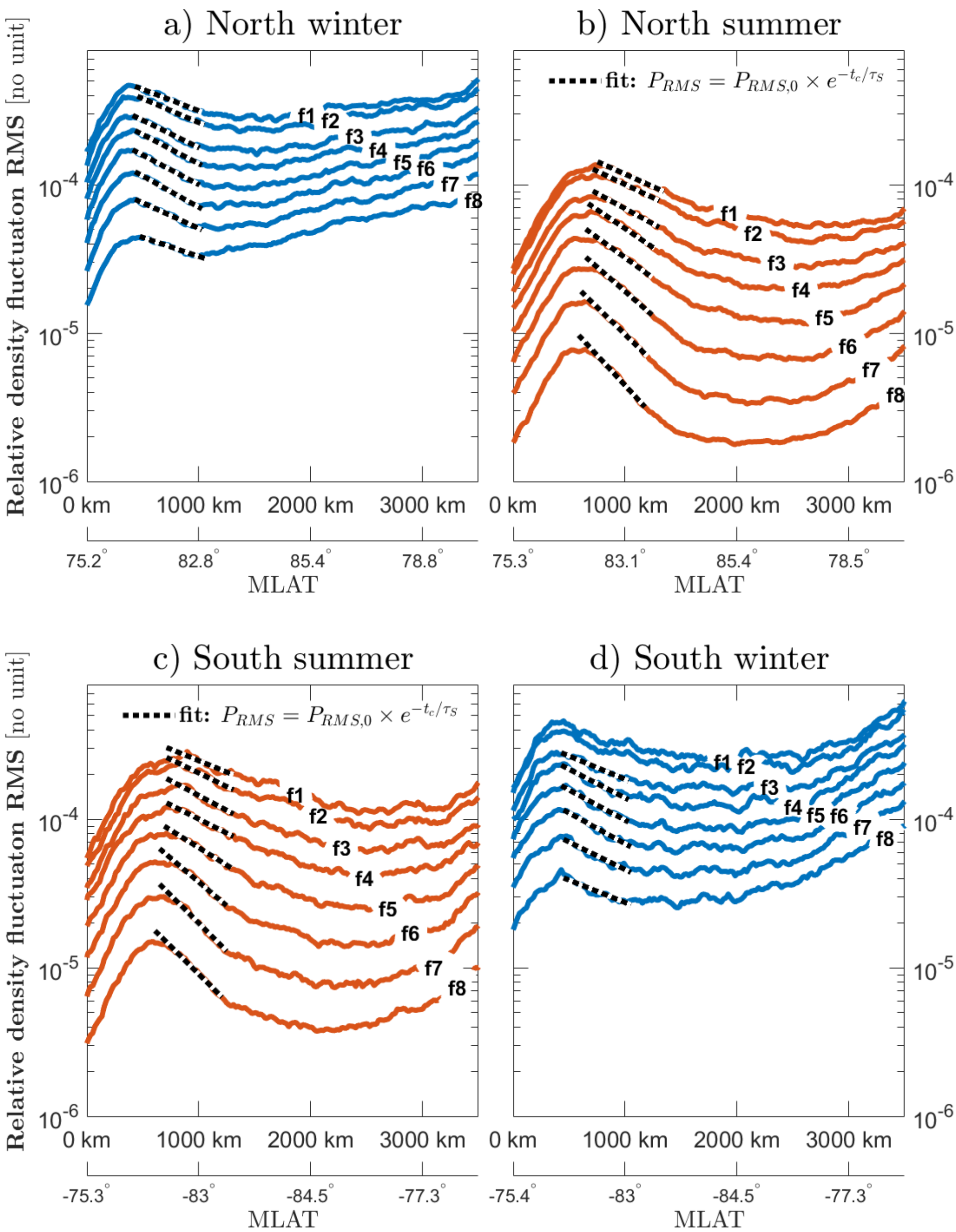

Figure 3. Plasma structure decay time estimates based on 16 Hz plasma density data from the Swarm A satellite. The top panels show the superposed epoch analysis for 1302 local winter passes (a) and 1144 local summer passes (b) through the northern polar cap, with both seasons defined by a 131-day window centered on the relevant solstice, for 8 frequency intervals. The bottom panels similarly show the superposed epoch analysis for 630 local winter passes (c) and 570 local summer passes (d). An exponential fit through 600 km of the assumed convection path of plasma through the polar cap is shown with dotted black lines (Eq. 7). The x-axes show both the underlying data magnetic latitudes, and the plasma convection distance (Eq. 4). The data used spans a time period from 2 Oct 2014 until 30 June 2019.

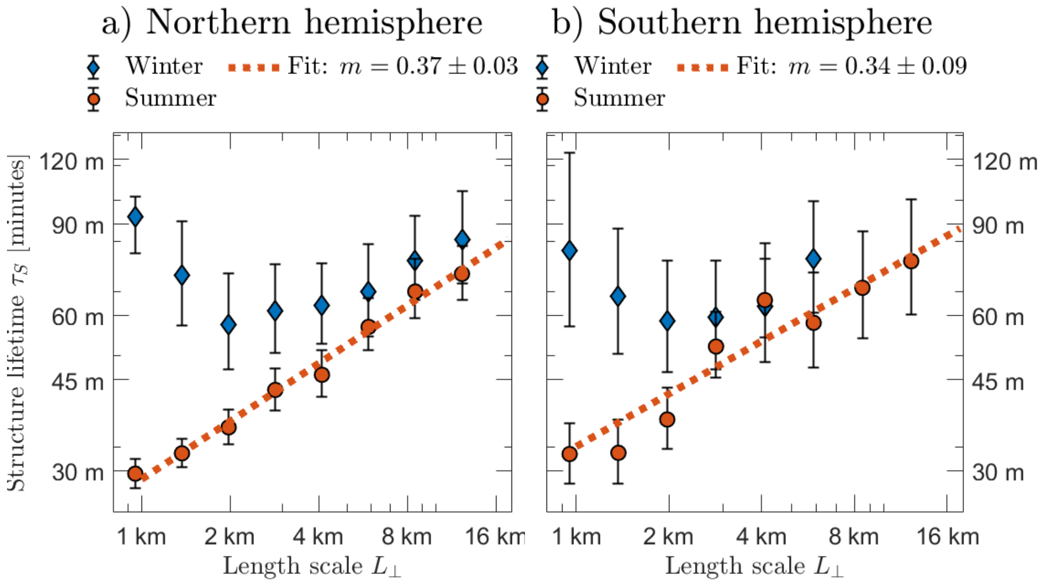

Figure 4. The scaling of the structure lifetime estimates, for local summer (orange) and local winter (blue), for both the northern (panel a) and southern (panel b) hemispheres. The structure lifetimes, shown on the y-axes, correspond to the exponential fits displayed in Fig. 3. The vertical errorbars are the 90 percent confidence intervals from a 10^4-iteration bootstrap routine. Fits of Eq. (16) are shown in orange dotted lines, and the exponent m is indicated aboeve (with error intervals corresponding to 90 percent confidence intervals of the fitting procedures).

In Fig. 3, we show the result of the superposed epoch analysis for the northern (panels a, b) and southern (panels c, d) hemispheres. Panels b) and c) contain data from local summer, while panels a) and d) contain data from local winter. Each panel shows the superposed values of P_{RMS} for the eight frequency intervals considered, with distance (Eq. 4) and magnetic latitude on the x-axis. In all four panels, a prominent peak exists near the cusp regions, for all frequency intervals. At some point after passing the geomagnetic pole, the plasma has entered the midnight sector, where production of plasma structures due to auroral precipitation might be more prevalent than diffusion. To estimate structure lifetime as outlined in the Methodology section, we fit Eq. (7) to each superposed P_{RMS} curve. That is, we fit an exponential curve through the polar cap, starting from a point after the peak near the cusp region, extending 600 km into the polar cap. Here, we assume a plasma convection velocity of 300 m/s, a reasonable velocity for the central polar cap (Grant et al., 1995; Thomas et al., 2015). Cases where the coefficient of determination, or r^2, of the fit is less than 0.9 are discarded, which stops the structure lifetime for the frequency intervals of f_1 and f_2 from being evaluated in the southern hemisphere winter. The characteristic time scale, τ_S, of the exponential fit reflects the expected structure lifetime of the fluctuations over the frequency interval in question, and is then the end-product of the superposed epoch analysis.

In Fig. 4, for the northern (panel a) and southern (panel b) hemispheres, we plot the structure lifetimes τ_S against the scale length $L_\perp$ at which the lifetime estimate was calculated. $L_\perp$ is calculated based on the assumption that the plasma convection velocity (assumed to be 300 m/s) is negligible compared to the velocity of Swarm A (7600 m/s). That is, $L_\perp(f) = v_S/f$, where f is the mean frequency of the frequency interval. See Table 1 for the eight scale lengths. Local winter structure times are shown in blue, while local summer is shown in orange. The vertical errorbars are 90-percent confidence intervals from a 10^4-iteration bootstrap routine. We see that while the local summer structure times exhibit a predictable behaviour with respect to the length scale $L_\perp$, the local winter structure times do not, exhibiting instead opposite behaviour for the smallest scales. Also shown, in a dotted orange line, is what amounts to a fit of Eq. (3). Here, we fit,

$$\tau_S = \frac{L_{\perp 0}^{2-m}}{D_S}\, L_\perp^m, \tag{16}$$

where D_S and m are fitting parameters determined using a non-linear least squares fitting procedure, and $L_{\perp 0}$ is a length scale equal to unity to ensure correct dimensionality in Eq. (16). The values of the exponent m are 0.36±0.04 and 0.35±0.09 for the northern and southern hemispheres respectively, with error intervals given by the 90-percent confidence interval of the fitting procedure. We now make an important observation: the values of the exponent m reported here are far from the $m = 2$ in Eq. (3). Since the scaling difference between λ of Eq. (3) and $L_\perp$ of Eq. (16) will not affect the the exponent m, we suggest that the discrepancy might be due to irregularity production and scale mixing, such as explained in the Introduction section. Consequently we cannot accurately estimate the field-perpendicular diffusion coefficient using in-situ data from Swarm, and the structure lifetime estimates presented here likely are higher than the theoretical decay lifetime for a given scale such as given by Eq. (3).

In Fig. 4, we see that the smallest scale, which corresponds to frequencies between 5.6 Hz and 8 Hz and has a scale length of 1.1 km, exhibits the largest seasonal contrast. To better understand this contrast, we construct a variable we refer to as wrapped day-of-year, D_w,

$$D_w = \begin{cases} 365 - D & \text{if } D > 365/2 \\ D & \text{otherwise,} \end{cases} \tag{17}$$

where D is the number of days elapsed since 1 January in the relevant year (day of year). We then make 9 overlapping bins with a window size of 65.5 days, from $D_w = [0, 65.5]$ to $D_w = [117, 182.5]$. For each bin, we repeat the superposed epoch analysis detailed above.To make a general prediction of 1.1 km-structure lifetimes in the central polar cap based on the ionospheric models, we solve Eq. (1 for each individual orbit that make up the superposed epoch analyses detailed above. We only include points directly under the exponential fits in Figs. 3 (roughly between ±78° and ±83° magnetic latitude). For each estimate of τ_S, we then have two additional observations, the Σ^E/Σ^F-ratio, and $\mathcal{D}_\perp$. As stated, we cannot use in-situ observations such as those presented here to estimate diffusion coefficient $\mathcal{D}_\perp$. We can, however, use Eq. (3) to calculate the decay time based on a given value of $\mathcal{D}_\perp$. According to Moisan and Pelletier (2012), for radial diffusion of cylindrical structures, $\lambda = L_\perp/2.405$. With this scaling, we can evaluate Eq. (3), to give an estimate of *decay time* (we remind the reader that we distinguish between τ_S, the effective structure lifetime, and τ, the theoretical decay time). For each D_w bin we then store the in-situ-based value of the 1.1 km-structure lifetime τ_S, and the model-based Σ^E/Σ^F-ratio, in addition to the model-based field-perpendicular diffusion coefficient $\mathcal{D}_\perp$.

In panels a) (northern hemisphere) and b) (southern hemisphere) of Fig. 5, we show the result of this joint analysis:

- In green triangle markers, we show the model-based decay time (left y-axis), versus Σ^E/Σ^F (x-axis). On the right y-axis, we show corresponding field-perpendicular diffusion coefficient $\mathcal{D}_\perp$ (inverted axis). Here, both vertical and horizontal errorbars represent the upper and lower quartile distributions in the underlying data. The values of τ for the 9 D_w bins correlate well with the Σ^E/Σ^F-ratio: the Pear-

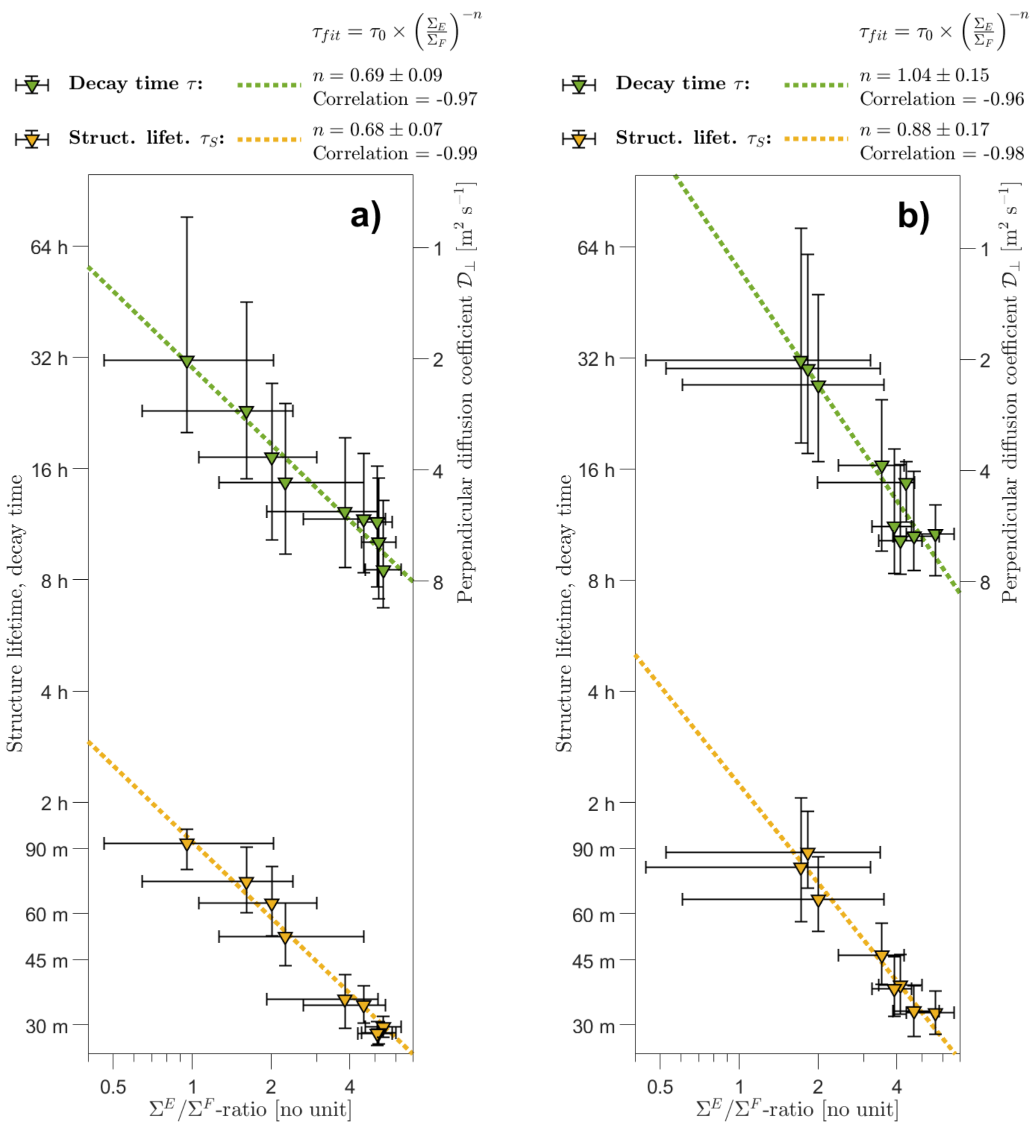

Figure 5. **Green:** Model-based decay time (left y-axis), based on the calculated $\mathcal{D}_\perp$ (right y-axis, inverted), versus Σ^E/Σ^F (x-axis), calculated for each individual orbit that make up the in-situ structure lifetime estimates above. Nine datapoints represent nine overlapping D_w bins (Eq. 17), ranging from the December solstice until the June solstice, each containing polar cap passes over a 131-day window, for the northern **(a)** and southern **(b)** hemispheres. For the model-based decay time, both vertical and horizontal errorbars represent the upper and lower quartile distributions in the underlying data. **Yellow:** Structure lifetime estimates for 1.1 km structures, versus the Σ^E/Σ^F-ratio, using in-situ data from Swarm A. Vertical errorbars are based on a bootstrap routine with 10^4 iterations (with a 90 percent confidence interval), and horizontal errorbars are based on the upper and lower quartile distribution of the underlying Σ^E/Σ^F data. For both the in-situ data (yellow dotted line), and the model-based data (green dotted line), we show a fit of Eq. (18), with the exponent n and the Pearson correlation coefficient indicated. All axes are in a $\log_{10}$ representation. Both the in-situ data and the model-based data covers the period from 14 October 2014 until 30 June 2019.

son correlation coefficient in this log-log representation measures -0.97 for the northern hemisphere and -0.96 for the southern hemisphere. Motivated by this high correlation, we fit a power law to data,

$$\tau_{\text{fit}} = \tau_0 \left(\frac{\Sigma^E}{\Sigma^F} \right)^{-n}, \tag{18}$$

where the free fitting variable τ_0 and the exponent n are determined by a nonlinear least-squares fitting procedure. Eq. (18) is shown in dotted green lines.

- In yellow triangle markers, we show the in-situ estimated 1.1 km-structure lifetimes for 9 bins between December and June solstice, with the value of Σ^E/Σ^F for each bin along the x-axis, where both the x- and y-axes are scaled logarithmically. Here, the errorbars along the x-axis are the lower and upper quartile distributions in each bin, while the errorbars along the y-axis are 90-percent confidence intervals from a 10^4-iteration bootstrap routine, performed on each D_w bin individually. In dotted yellow lines, we show a fit of Eq. (18), with the Pearson correlation coefficient indicated. The in-situ-based τ_S likewise correlate well with the Σ^E/Σ^F-ratio, exhibiting correlation coefficients of -0.99 and -0.98 for the northern and southern hemispheres respectively.

We immediately make an important observation: the values of the diffusion coefficient $\mathcal{D}_\perp$ as predicted by the ionospheric models are substantially lower than the $\propto 10^2$ m s^{-2} that are reported in the literature. This leads to very high values of decay time τ, several times higher than the in-situ structure lifetime estimates. However, a clear dependency of τ on Σ^E/Σ^F can still be gleaned from the data. This dependency is strikingly similar between the in-situ and the model-based data. In the northern hemisphere, $n = 0.68 \pm 0.09$ for the in-situ data and $n = 0.69 \pm 0.11$ for the model-based data. In the southern hemisphere, for the exponent n, we find that $n = 0.88 \pm 0.21$ for the in-situ data and $n = 1.04 \pm 0.19$ for the model-based data. The error intervals in n are given by 90-percent confidence intervals of the fitting procedure.

4 Discussion

In Fig. 4, there are several interesting observations to be made. First, the estimated structure lifetime τ_S increases with structure scale for local summer, where a powerlaw with exponent around 0.35 describes the scale-dependency of structure lifetime, with both hemispheres in clear agreement. The exponent deviates from that of the theoretical prediction (exponent valued at 2, Eq. 3). This is consistent with simultaneous diffusion occurring on a range of scales, where the diffusion of smaller scales contribute negatively to the diffusion of larger scales, increasing the effective decay time on all scales (see the schematic Fig. 1). Second, for both hemispheres, the local summer and winter lifetimes are indistinguishable for scales larger than around 4 km. This scale matches the scale at which Keskinen and Huba (1990) found that high-latitude plasma irregularities should transition to a fully collisional regime. Third, the local winter structure times do not, for the most part, decrease linearly with decreasing scale. We interpret this as an indication that small-scale (~ 1 km) diffusion during local winter is significantly reduced, which can explain the reported increase in local winter plasma irregularities (Heppner et al., 1993; Ghezelbash et al., 2014; Prikryl et al., 2015; Jin et al., 2017, 2018) Additionally, Ivarsen et al. (2019) found that only 20 % of local winter PSD spectra exhibits evidence for diffusion, while, conversely, 80 % of local summer spectra does so. It is then not surprising that we were not able to infer diffusion during local winter. For scales around 5 km, we find that the structure lifetimes are indistinguishable between local winter and local summer. In Ivarsen et al. (2019), we found direct evidence for diffusion occurring for scales on average lower than 5.8 km, which might then constitute an upper boundary for detectable diffusion in the Swarm 16 Hz plasma density data set.

In Fig. 5, we see that there is a large spread in the Σ^E/Σ^F values, and that the southern hemisphere exhibits a shorter range and larger spread in the Σ^E/Σ^F-ratio, decay time, and structure lifetimes compared to the northern hemisphere. Nevertheless, in both hemispheres the data tend to fall on the same straight line in a log-log representation. The in-situ-estimated structure lifetimes τ_S correlate well with the simultaneous model-based Σ^E/Σ^F-ratio. They show correlation coefficients of -0.99 for the northern hemisphere, and -0.98 for the southern hemisphere, which matches the correlation between the model-based decay time τ and the Σ^E/Σ^F-ratio. This is a strong indicator that the model first proposed by Vickrey and Kelley (1982) is suitable, and that the ratio of E-region to F-region conductance to a large degree predicts F-region diffusion rates, and thus the occurrence of plasma irregularities in the polar caps.

However, the reported agreement in how both the in-situ based τ_S and the model-based τ respond to the Σ^E/Σ^F-ratio is only valid for the smallest scales available to investigation using the Swarm 16 Hz plasma density data. There is a scale-dependency in the observable plasma diffusion in the polar caps, with diffusion primarily being observed on scales smaller than a threshold particular to local conditions (Ivarsen et al., 2019). Based on this, and the fact that the smallest scales available are fairly close to the characteristic scale at which the irregularities should transition to a fully collisional regime (Keskinen & Huba, 1990), we believe the use of higher resolution plasma density data is necessary to further our knowledge about ionospheric plasma structure lifetimes. In addition, the analysis presented here is sensitive to the assumed polar cap convection velocity. In future investigations of plasma structure lifetimes, special care should be taken in treating plasma convection velocity, e.g. by using methods of observing plasma drift velocity (Park et al., 2015).

We now draw the reader's attention to the large discrepancy between the in-situ based structure lifetimes τ_S and the model-based decay times τ: the models employed in the present study predict a much lower perpendicular diffusion coefficient than is realistic in the polar caps, with several studies utilizing ground-based radar measurements indicating that $\mathcal{D}_\perp \propto 10^2$ (Gresillon et al., 1992; Villain et al., 1996; André et al., 2003). We will now address this discrepancy, and suggest a possible solution.

In several laboratory experiments, the theorized classical value of perpendicular diffusion coefficient has not been sufficiently high to explain observed diffusion rates. During the last 70 years researchers have referred to the observed high diffusion rates as *anomalous* diffusion, and have often resorted to ascribing it to Bohm diffusion (Braginskii, 1965; Hockney, 1966; Okuda et al., 1972; Okuda & Dawson, 1973; Millar, 1976; Marchetti et al., 1984; Kaufman, 1990; Ott & Bonitz, 2011; Curreli & Chen, 2014). Bohm diffusion, or Bohm-like diffusion, which theoretically applies to the diffusion of ions (e.g., Spitzer, 1960; Kaufman, 1990), is defined as,

$$D_B = \gamma \frac{k_B T}{eB}, \tag{19}$$

where T is the plasma temperature of either ions or electrons (Spitzer, 1960). In Eq. (19), γ is a numerical factor first set to 1/16, but which has since been found through several experiments to in effect be higher (e.g., Ott & Bonitz, 2011). Crucially, $D_B \propto B^{-1}$, meaning that for cross-field diffusion, $D_B \gg D_{\perp,i}$. Since cross-field plasma diffusion is vital in the field of plasma fusion energy production, many attempts have been made to explain why Bohm-like diffusion is frequently observed (Kaufman, 1990; Ott & Bonitz, 2011). Early simulations showed that Bohm diffusion can be observed in collisionless plasma (Hockney, 1966), indicating that it is independent of collisionally induced diffusion. In fact, it has been shown that while collisional diffusion across the magnetic field adhere to $\propto B^{-2}$, convection-induced diffusion follows the Bohm-like $\propto B^{-1}$ (Okuda et al., 1972). This second regime is associated with strong applied magnetic fields (Marchetti et al., 1984; Deutsch & Popoff, 2009; Ott & Bonitz, 2011). Furthermore, observations of Bohm-like diffusion have been linked to inhomogeneties in the plasma density and magnetic field strength (Okuda & Dawson, 1973; Millar, 1976; Ott & Bonitz, 2011).

Most polar cap plasma irregularities are due to instability processes in the plasma gradients associated with polar cap patches (Tsunoda, 1988; Jin et al., 2019). In such turbulent processes, Bohm diffusion might be present (Braginskii, 1965). We suggest that Bohm-like diffusion accounts for the discrepancy between observations and the model-based results. Indeed, more recently, St-Maurice and Hamza (2009) and Villain et al. (1996) both argue that ionospheric turbulence can induce Bohm-like diffusion.

However, the theoretical application of Bohm diffusion is not straightforward. In the literature, several authors add a Bohm-like diffusion term, D_B, to the classical diffusion coefficient (Okuda et al., 1972; Millar, 1976; Marchetti et al., 1984; Deutsch & Popoff, 2009):

$$D_{\perp,i} = \frac{D_{0,i}\nu_i^2}{\omega_i^2 + \nu_i^2} + D_B, \tag{20}$$

By using Eq. (19) with $T = T_i$ when evaluating the model-based perpendicular ion diffusion, the models applied in the present study tend to yield perpendicular diffusion coefficients in the range $[10^1, 10^2]$, roughly in agreement with ground-based radar measurements (Gresillon et al., 1992; Villain et al., 1996; André et al., 2003). However, many uncertainties remain regarding Bohm diffusion and how it applies to the free diffusion of ions and electrons. We suspect that ionospheric Bohm diffusion is also controlled by the ratio of E- to F-region conductance, ensuring a relative absence of Bohm diffusion during local winter. However, to the authors' best knowledge, there are no first-principles derivation of how electron and ion Bohm diffusion should be treated separately, and so a rigorous application of Bohm diffusion to ionospheric plasma diffusion is outside the scope of the present study.

5 Conclusion

In this study we have approached the subject of field-perpendicular plasma diffusion and field-perpendicular plasma structure lifetimes from two angles. By using almost 5 years of in-situ data from Swarm A, and by applying ionospheric models, we have made several new observations regarding structure lifetimes, decay time, and their seasonal dependencies. Both the in-situ data and the ionospheric models support the claim that perpendicular diffusion in the F-region polar caps is highly dependent on the relationship between E- and F-region conductances.

Our results indicate that while the propagation of small-scale ($<$ 4 km) structure is virtually uninhibited during local winter, we are able to observe the characteristics of local summer diffusion in both the northern and southern polar caps. This leads to, for the first time as far the authors are aware, a systematic prediction of small scale structure lifetimes in the F-region polar caps. We find that for the smallest scale investigated, which corresponds to frequencies between 5.6 Hz and 8 Hz, with a scale length of 1.1 km, structure lifetimes range from 30 minutes during local summer to around 90 minutes during local winter. Although the seasonal contrast in plasma structure time harmonizes with reported seasonal dependencies in polar cap plasma irregularities, more work is needed to estimate plasma structure times more accurately, e.g. by using higher resolution plasma density data.

There is a large discrepancy in the perpendicular diffusion coefficient between the models and the ground-based radar estimates reported in the literature, as well as a discrepancy between the in-situ-estimated structure lifetimes and the model-based decay times. We suggest that this discrepancy can be explained by anomalous (or Bohm) diffusion. However more work remains to be done in working out the details of exactly how anomalous diffusion is induced in ionospheric plasma.

Acknowledgments

The authors acknowledge ESA for the provision of the Swarm data, which was accessed from `ftp://swarm-diss.eo.esa.int/`. The authors would like to extend thanks to D. J. Knudsen, J. K. Burchill, and S. C. Buchert for their work on the Swarm Thermal ion imager instrument. The authors are grateful to I. Ivarsen for proofreading. This work is a part of the 4DSpace initiative at the University of Oslo.

References

André, R., Hanuise, C., Villain, J.-P., & Krasnoselskikh, V. (2003, August). Turbulence characteristics inside ionospheric small-scale expanding structures observed with SuperDARN HF radars. *Annales Geophysicae*, *21*(8), 1839–1845. Retrieved 2019-12-19, from `https://www.ann-geophys.net/21/1839/2003/` doi: https://doi.org/10.5194/angeo-21-1839-2003

Basu, S., MacKenzie, E., & Basu, S. (1988, May). Ionospheric constraints on VHF/UHF communications links during solar maximum and minimum periods. *Radio Science*, *23*(3), 363–378. Retrieved 2018-09-02, from `https://agupubs.onlinelibrary.wiley.com/doi/abs/10.1029/RS023i003p00363` doi: 10.1029/RS023i003p00363

Bilitza, D., Altadill, D., Zhang, Y., Mertens, C., Truhlik, V., Richards, P., ... Reinisch, B. (2014). The International Reference Ionosphere 2012 a model of international collaboration. *Journal of Space Weather and Space Climate*, *4*, A07. Retrieved 2018-06-13, from `https://www.swsc-journal.org/articles/swsc/abs/2014/01/swsc130043/swsc130043.html` doi: 10.1051/swsc/2014004

Bilitza, D., & Reinisch, B. W. (2008, August). International Reference Ionosphere 2007: Improvements and new parameters. *Advances in Space Research*, *42*(4), 599–609. Retrieved 2018-06-13, from `http://www.sciencedirect.com/science/article/pii/S0273117708000288` doi: 10.1016/j.asr.2007.07.048

Braginskii, S. I. (1965). Transport Processes in a Plasma. *Reviews of Plasma Physics*, *1*, 205. Retrieved 2020-02-27, from `http://adsabs.harvard.edu/abs/1965RvPP....1..205B`

Coley, W. R., & Heelis, R. A. (1998, February). Structure and occurrence of polar ionization patches. *Journal of Geophysical Research: Space Physics*, *103*(A2), 2201–2208. Retrieved 2018-09-06, from `https://agupubs.onlinelibrary.wiley.com/doi/abs/10.1029/97JA03345` doi: 10.1029/97JA03345

Cowley, S. W. H. (2000). TUTORIAL: Magnetosphere-Ionosphere Interactions: A Tutorial Review. *Washington DC American Geophysical Union Geophysical Monograph Series*, *118*, 91. Retrieved 2018-03-07, from `http://adsabs.harvard.edu/abs/2000GMS...118...91C` doi: 10.1029/GM118p0091

Cowley, S. W. H., & Lockwood, M. (1992, February). Excitation and decay of solar wind-driven flows in the magnetosphere-ionosphere system. *Annales Geophysicae*, *10*, 103–115. Retrieved 2018-03-07, from `http://adsabs.harvard.edu/abs/1992AnGeo..10..103C`

Curreli, D., & Chen, F. F. (2014, October). Cross-field diffusion in low-temperature plasma discharges of finite length. *Plasma Sources Science and Technology*, *23*(6), 064001. Retrieved 2019-08-31, from `https://doi.org/10.1088%2F0963-0252%2F23%2F6%2F064001` doi: 10.1088/0963-0252/23/6/064001

Danskin, D. W., Koustov, A. V., Ogawa, T., Nishitani, N., Nozawa, S., Milan, S. E., ... Andre, D. (2002, September). On the factors controlling occurrence of

F-region coherent echoes. *Annales Geophysicae*, *20*(9), 1385–1397. Retrieved 2019-02-18, from https://www.ann-geophys.net/20/1385/2002/ doi: https://doi.org/10.5194/angeo-20-1385-2002

Deutsch, C., & Popoff, R. (2009, July). Low ion velocity slowing down in a strongly magnetized plasma target. *Nuclear Instruments and Methods in Physics Research Section A: Accelerators, Spectrometers, Detectors and Associated Equipment*, *606*(1), 212–214. Retrieved 2019-09-03, from http://www.sciencedirect.com/science/article/pii/S0168900209005786 doi: 10.1016/j.nima.2009.03.100

Dungey, J. W. (1961, January). Interplanetary Magnetic Field and the Auroral Zones. *Physical Review Letters*, *6*, 47–48. Retrieved 2018-03-08, from http://adsabs.harvard.edu/abs/1961PhRvL...6...47D doi: 10.1103/PhysRevLett.6.47

Foster, J. C. (1984, February). Ionospheric signatures of magnetospheric convection. *Journal of Geophysical Research: Space Physics*, *89*(A2), 855–865. Retrieved 2018-09-06, from https://agupubs.onlinelibrary.wiley.com/doi/abs/10.1029/JA089iA02p00855 doi: 10.1029/JA089iA02p00855

Friis-Christensen, E., Lhr, H., & Hulot, G. (2006, April). Swarm: A constellation to study the Earths magnetic field. *Earth, Planets and Space*, *58*, BF03351933. doi: 10.1186/BF03351933

Ghezelbash, M., Koustov, A. V., Themens, D. R., & Jayachandran, P. T. (2014, December). Seasonal and diurnal variations of PolarDARN F region echo occurrence in the polar cap and their causes. *Journal of Geophysical Research: Space Physics*, *119*(12), 10,426–10,439. Retrieved 2018-09-03, from https://agupubs.onlinelibrary.wiley.com/doi/abs/10.1002/2014JA020726 doi: 10.1002/2014JA020726

Grant, I. F., MacDougall, J. W., Ruohoniemi, J. M., Bristow, W. A., Sofko, G. J., Koehler, J. A., … André, D. (1995). Comparison of plasma flow velocities determined by the ionosonde Doppler drift technique, SuperDARN radars, and patch motion. *Radio Science*, *30*(5), 1537–1549. Retrieved 2020-02-24, from https://agupubs.onlinelibrary.wiley.com/doi/abs/10.1029/95RS00831 doi: 10.1029/95RS00831

Gresillon, D., Cabrit, B., Villain, J. P., Hanuise, C., Truc, A., Laviron, C., … Devynck, P. (1992, December). Collective scattering of electromagnetic waves and cross-B plasma diffusion. *Plasma Physics and Controlled Fusion*, *34*(13), 1985–1991. Retrieved 2019-12-18, from https://doi.org/10.1088%2F0741-3335%2F34%2F13%2F030 doi: 10.1088/0741-3335/34/13/030

Heppner, J. P., Liebrecht, M. C., Maynard, N. C., & Pfaff, R. F. (1993, February). High-latitude distributions of plasma waves and spatial irregularities from DE 2 alternating current electric field observations. *Journal of Geophysical Research: Space Physics*, *98*(A2), 1629–1652. Retrieved 2018-09-06, from https://agupubs.onlinelibrary.wiley.com/doi/abs/10.1029/92JA01836 doi: 10.1029/92JA01836

Hockney, R. W. (1966, September). Computer Experiment of Anomalous Diffusion. *The Physics of Fluids*, *9*(9), 1826–1835. Retrieved 2019-08-31, from https://aip.scitation.org/doi/10.1063/1.1761939 doi: 10.1063/1.1761939

Huba, J. D., & Ossakow, S. L. (1981). Diffusion of small-scale density irregularities during equatorial spread F. *Journal of Geophysical Research: Space Physics*, *86*(A11), 9107–9114. Retrieved 2020-02-17, from https://agupubs.onlinelibrary.wiley.com/doi/abs/10.1029/JA086iA11p09107 doi: 10.1029/JA086iA11p09107

Ivarsen, M. F., Jin, Y., Spicher, A., & Clausen, L. B. N. (2019). Direct Evidence for the Dissipation of Small-Scale Ionospheric Plasma Structures by a Conductive E Region. *Journal of Geophysical Research: Space Physics*, *124*(4), 2935–2942. Retrieved 2019-09-12, from https://agupubs.onlinelibrary.wiley.com/

doi/abs/10.1029/2019JA026500 doi: 10.1029/2019JA026500

Jin, Y., Miloch, W. J., Moen, J. I., & Clausen, L. B. N. (2018). Solar cycle and seasonal variations of the GPS phase scintillation at high latitudes. *Journal of Space Weather and Space Climate*, *8*, A48. Retrieved 2018-11-22, from https:/articles/swsc/abs/2018/01/swsc170089/swsc170089.html doi: 10.1051/swsc/2018034

Jin, Y., Moen, J. I., Oksavik, K., Spicher, A., Clausen, L. B. N., & Miloch, W. J. (2017). GPS scintillations associated with cusp dynamics and polar cap patches. *Journal of Space Weather and Space Climate*, *7*, A23. Retrieved 2018-09-14, from https://www.swsc-journal.org/articles/swsc/abs/2017/01/swsc170040/swsc170040.html doi: 10.1051/swsc/2017022

Jin, Y., Spicher, A., Xiong, C., Clausen, L. B. N., Kervalishvili, G., Stolle, C., & Miloch, W. J. (2019). Ionospheric Plasma Irregularities Characterized by the Swarm Satellites: Statistics at High Latitudes. *Journal of Geophysical Research: Space Physics*, *124*(2), 1262–1282. Retrieved 2020-01-20, from https://agupubs.onlinelibrary.wiley.com/doi/abs/10.1029/2018JA026063 doi: 10.1029/2018JA026063

Kaufman, H. R. (1990, January). Explanation of Bohm diffusion. *Journal of Vacuum Science & Technology B: Microelectronics Processing and Phenomena*, *8*(1), 107–108. Retrieved 2019-08-30, from https://avs.scitation.org/doi/abs/10.1116/1.584855 doi: 10.1116/1.584855

Kelley, M. C., Vickrey, J. F., Carlson, C. W., & Torbert, R. (1982, June). On the origin and spatial extent of high-latitude F region irregularities. *Journal of Geophysical Research: Space Physics*, *87*(A6), 4469–4475. Retrieved 2018-09-03, from https://agupubs.onlinelibrary.wiley.com/doi/abs/10.1029/JA087iA06p04469 doi: 10.1029/JA087iA06p04469

Keskinen, M. J., & Huba, J. D. (1990, September). Nonlinear evolution of high-latitude ionospheric interchange instabilities with scale-size-dependent magnetospheric coupling. *Journal of Geophysical Research: Space Physics*, *95*(A9), 15157–15166. Retrieved 2018-03-05, from http://onlinelibrary.wiley.com/doi/10.1029/JA095iA09p15157/abstract doi: 10.1029/JA095iA09p15157

Kivanc, , & Heelis, R. A. (1998, April). Spatial distribution of ionospheric plasma and field structures in the high-latitude F region. *Journal of Geophysical Research*, *103*, 6955–6968. Retrieved 2018-08-13, from http://adsabs.harvard.edu/abs/1998JGR...103.6955K doi: 10.1029/97JA03237

Knudsen, D. J., Burchill, J. K., Buchert, S. C., Eriksson, A. I., Gill, R., Wahlund, J.-E., . . . Moffat, B. (2017, February). Thermal ion imagers and Langmuir probes in the Swarm electric field instruments. *Journal of Geophysical Research: Space Physics*, *122*(2), 2016JA022571. Retrieved 2018-03-07, from http://onlinelibrary.wiley.com/doi/10.1002/2016JA022571/abstract doi: 10.1002/2016JA022571

Marchetti, M. C., Kirkpatrick, T. R., & Dorfman, J. R. (1984, May). Anomalous diffusion of charged particles in a strong magnetic field. *Physical Review A*, *29*(5), 2960–2962. Retrieved 2019-08-31, from https://link.aps.org/doi/10.1103/PhysRevA.29.2960 doi: 10.1103/PhysRevA.29.2960

Milan, S. E., Davies, J. A., & Lester, M. (1999). Coherent HF radar backscatter characteristics associated with auroral forms identified by incoherent radar techniques: a comparison of CUTLASS and EISCAT observations. *Journal of Geophysical Research: Space Physics*, *104*(A10), 22591–22604.

Millar, D. D. (1976, August). Ion currents, ion-neutral collisions and plasma transport phenomena. *Australian Journal of Physics*, *29*, 249–261. Retrieved 2019-09-01, from http://adsabs.harvard.edu/abs/1976AuJPh..29..249M doi: 10.1071/PH760249

Moisan, M., & Pelletier, J. (2012). Hydrodynamic Description of a Plasma. In M. Moisan & J. Pelletier (Eds.), *Physics of Collisional Plasmas: Introduction* *to High-Frequency Discharges* (pp. 203–335). Dordrecht: Springer Netherlands. Retrieved 2019-09-02, from https://doi.org/10.1007/978-94-007-4558-2_3 doi: 10.1007/978-94-007-4558-2_3

Okuda, H., & Dawson, J. M. (1973, March). Theory and numerical simulation on plasma diffusion across a magnetic field. *The Physics of Fluids*, *16*(3), 408–426. Retrieved 2019-08-31, from https://aip.scitation.org/doi/abs/10.1063/1.1694356 doi: 10.1063/1.1694356

Okuda, H., Dawson, J. M., & Hooke, W. M. (1972, December). Interpretation of an Enhanced Diffusion Observed in a Solid-State Plasma. *Physical Review Letters*, *29*(25), 1658–1661. Retrieved 2019-09-01, from https://link.aps.org/doi/10.1103/PhysRevLett.29.1658 doi: 10.1103/PhysRevLett.29.1658

Ott, T., & Bonitz, M. (2011, September). Diffusion in a Strongly Coupled Magnetized Plasma. *Physical Review Letters*, *107*(13), 135003. Retrieved 2019-08-30, from https://link.aps.org/doi/10.1103/PhysRevLett.107.135003 doi: 10.1103/PhysRevLett.107.135003

Park, J., Lhr, H., Stolle, C., Malhotra, G., B. H. Baker, J., Buchert, S., & Gill, R. (2015, July). Estimating along-track plasma drift speed from electron density measurements by the three Swarm satellites. *Annales Geophysicae*, *33*, 829–835. doi: 10.5194/angeo-33-829-2015

Picone, J. M., Hedin, A. E., Drob, D. P., & Aikin, A. C. (2002). NRLMSISE-00 empirical model of the atmosphere: Statistical comparisons and scientific issues. *Journal of Geophysical Research: Space Physics*, *107*(A12), SIA 15–1–SIA 15–16. Retrieved 2019-09-02, from https://agupubs.onlinelibrary.wiley.com/doi/abs/10.1029/2002JA009430 doi: 10.1029/2002JA009430

Prikryl, P., Jayachandran, P. T., Chadwick, R., & Kelly, T. D. (2015, May). Climatology of GPS phase scintillation at northern high latitudes for the period from 2008 to 2013. *Ann. Geophys.*, *33*(5), 531–545. Retrieved 2018-09-13, from https://www.ann-geophys.net/33/531/2015/ doi: 10.5194/angeo-33-531-2015

Schunk, R. W., & Nagy, A. F. (1980). Ionospheres of the terrestrial planets. *Reviews of Geophysics*, *18*(4), 813–852. Retrieved 2019-09-02, from https://agupubs.onlinelibrary.wiley.com/doi/abs/10.1029/RG018i004p00813 doi: 10.1029/RG018i004p00813

Schunk, R. W., & Sojka, J. J. (1987, November). A theoretical study of the lifetime and transport of large ionospheric density structures. *Journal of Geophysical Research: Space Physics*, *92*(A11), 12343–12351. Retrieved 2018-09-06, from https://agupubs.onlinelibrary.wiley.com/doi/abs/10.1029/JA092iA11p12343 doi: 10.1029/JA092iA11p12343

Spicher, A., Clausen, L. B. N., Miloch, W. J., Lofstad, V., Jin, Y., & Moen, J. I. (2017, March). Interhemispheric study of polar cap patch occurrence based on Swarm in situ data. *Journal of Geophysical Research: Space Physics*, *122*(3), 3837–3851. Retrieved 2018-09-07, from https://agupubs.onlinelibrary.wiley.com/doi/abs/10.1002/2016JA023750 doi: 10.1002/2016JA023750

Spitzer, L. (1960, July). Particle Diffusion across a Magnetic Field. *The Physics of Fluids*, *3*(4), 659–661. Retrieved 2019-09-02, from https://aip.scitation.org/doi/10.1063/1.1706104 doi: 10.1063/1.1706104

St-Maurice, J.-P., & Hamza, A. M. (2009). Small scale irregularities at high latitudes. In *Characterising the Ionosphere, ed. G. Wyman; Technical Report RTO-TR-IST-051.* Neuilly-sur-Seine, France: RTO.

Thomas, E. G., Hosokawa, K., Sakai, J., Baker, J. B. H., Ruohoniemi, J. M., Taguchi, S., ... McWilliams, K. A. (2015). Multi-instrument, high-resolution imaging of polar cap patch transportation. *Radio Science*, *50*(9), 904–915. Retrieved 2020-02-24, from https://agupubs.onlinelibrary.wiley.com/doi/abs/10.1002/2015RS005672 doi: 10.1002/2015RS005672

Thébault, E., Finlay, C. C., Beggan, C. D., Alken, P., Aubert, J., Barrois, O., . . . Zvereva, T. (2015, May). International Geomagnetic Reference Field: the 12th generation. *Earth, Planets and Space*, *67*(1), 79. Retrieved 2019-09-02, from https://doi.org/10.1186/s40623-015-0228-9 doi: 10.1186/s40623-015-0228-9

Tsunoda, R. T. (1988, November). High-latitude F region irregularities: A review and synthesis. *Reviews of Geophysics*, *26*(4), 719–760. Retrieved 2018-03-07, from http://onlinelibrary.wiley.com/doi/10.1029/RG026i004p00719/abstract doi: 10.1029/RG026i004p00719

Vickrey, J. F., & Kelley, M. C. (1982, June). The effects of a conducting E layer on classical F region cross-field plasma diffusion. *Journal of Geophysical Research: Space Physics*, *87*(A6), 4461–4468. Retrieved 2018-03-06, from http://onlinelibrary.wiley.com/doi/10.1029/JA087iA06p04461/abstract doi: 10.1029/JA087iA06p04461

Villain, J. P., André, R., Hanuise, C., & Grésillon, D. (1996, June). Observation of the high latitude ionosphere by HF radars: interpretation in terms of collective wave scattering and characterization of turbulence. *Journal of Atmospheric and Terrestrial Physics*, *58*(8), 943–958. Retrieved 2019-12-18, from http://www.sciencedirect.com/science/article/pii/0021916995001255 doi: 10.1016/0021-9169(95)00125-5

Wood, A. G., & Pryse, S. E. (2010, July). Seasonal influence on polar cap patches in the high-latitude nightside ionosphere. *Journal of Geophysical Research: Space Physics*, *115*(A7). Retrieved 2018-09-03, from https://agupubs.onlinelibrary.wiley.com/doi/abs/10.1029/2009JA014985 doi: 10.1029/2009JA014985